Microchemical Journal 207 (2024) 112015

Contents lists available at ScienceDirect

Microchemical Journal

journal homepage: www.elsevier.com/locate/microc

Self-seal laser ablation open cell for trace elements analysis of full-size archaeological artefacts: Application on *Famille Rose* enamel

Thomas Delbey [a,*], Dana Norris [a,b], David Douglas [c], Andrew Shortland [a]

[a] Cranfield Forensic Institute, Cranfield University, Defence Academy of The United Kingdom, Shrivenham SN6 8LA, United Kingdom
[b] Victoria and Albert Museum Cromwell Rd, London, England SW7 2SL, United Kingdom
[c] Elemental Scientific Lasers LLC, Bozeman, Montana, United States

ARTICLE INFO

Keywords:
LA-ICP-MS
Open cell
Trace elements analysis
Chinese enamel
Famille Rose
Heritage science

ABSTRACT

Laser Ablation Inductively Coupled Plasma Mass Spectrometry (LA-ICP-MS) is a technique that is increasingly becoming the standard analytical approach in archaeological science, especially for the analysis of glass, glaze, and metal. Its low detection limits, high precision and wide element range is twinned with a very small sample size, which makes it ideal for culturally valuable objects. However, in the past, the small sample chamber size in commercial laser systems has meant that the size of object that could be analysed is very limited. Ongoing work by various groups has demonstrated the potential of open architecture and portable systems to overcome this issue. This paper reports an example of this – the results of a validation on a self-seal open ablation cell coupled with a very large sample chamber developed by Cranfield University and Elemental Scientific Lasers LLC. Comparison of the analysis of standard reference materials between the self-seal open cell and a conventional closed cell in a two-volume chamber show that, the count rates for most elements drop in the open cell to between 40–70% with our configuration, but precision, accuracy, fractionation, and limits of detection are barely affected. This means that the result outputs of both chambers are very similar and shows that the open cell is a very real solution to the problem of the small sample chambers in conventional LA-ICP-MS facilities.

The functionality of the open cell is demonstrated using a case study of two Chinese, polychrome enamelled copperwares dating from the late 18th or early 19th century Qianlong or Jiaqing period, a tray and a writing set. Due to conservation work on the pieces, five small enamel samples were available, which meant that the results derived from these samples in the conventional laser chamber could be compared to results from the objects themselves in the large sample chamber. Time resolved analysis was carried out giving more information on the thickness of enamel layers and variability between colours and across the object demonstrating the usefulness of having large, complete objects in the chamber.

1. Introduction

Laser Ablation Inductively Coupled Plasma Mass Spectrometry (LA-ICP-MS) can be considered as a mature analytical technique often applied for trace and ultra-trace elements quantification in archaeological and historical artefacts [1]. It is widely used on various types of materials such as glass, ceramic, and metal for provenance analysis, material characterization, reconstitution of ancient technology, and conservation research. The successful development of this method can be explained by its quasi-non-destructive character, the wide array of elements analysed, the low detection limit and the relatively short time of analysis.

The instrument is uniquely suited to the study of art and archaeological objects made in vitreous materials (ceramics, glass, and enamels) which can be disfigured by inappropriate sampling. Instead, with LA-ICP-MS microscopic areas of the surface can be ablated to identify and quantify key elements in enamels and glass some of which are below the limit of detection or difficult to measure accurately with other techniques. LA-ICP-MS is considered minimally destructive because ablation creates very small pits on the surface. Ablation pits often go unnoticed to the naked eye and resemble pin hole type firing faults, ideal for the study of rare and high-status objects. However, in a conventional set up, research is curtailed by the dimensions of the object to analyse which have to fit in the ablation chamber (typically 100 mm X 100 mm and 30

* Corresponding author.
E-mail address: thomas.delbey@cranfield.ac.uk (T. Delbey).

https://doi.org/10.1016/j.microc.2024.112015
Received 24 June 2024; Received in revised form 21 October 2024; Accepted 23 October 2024
Available online 28 October 2024
0026-265X/© 2024 The Authors. Published by Elsevier B.V. This is an open access article under the CC BY license (http://creativecommons.org/licenses/by/4.0/).

mm deep working area in a standard TwoVol2 ablation chamber).

Several laser ablation sampling strategies have been developed to prevent the destructive sub-sampling of objects to match the size of the ablation chamber. The so-called open cell approach makes use of an ablation cell which is not encased in an airtight chamber and can be placed above the surface of the sample regardless of its size. A flexible and straightforward sampling method used a sealing system to create a small airtight ablation cell where the surface of the sample is in contact with the walls of the cell (this design is sometimes called "half open cell" in comparison with the contactless laser ablation system). In this type of design, plasticine or plastic adhesive have been used to ensure the quality of the sealing. The carrier gas is injected by a nozzle in the cell and the aerosol is then steered directly to the ICP-MS [2,3]. In-house built systems using sealed open cells have been used in heritage science case studies to investigate the composition of historical paintings [4] and archaeological ceramics [5,6] (using the same laser ablation system).

A second type of open cell design includes a laser ablation cell using an annular gas flow (argon or nitrogen) to entrain the aerosol to the ICP-MS. The early designs of this type of cell allowing contactless analysis were contained in a box pressurised with argon [7,8]. This system has been improved by Asogan et al. (2009) [9] using a dual concentric annular gas flow to exclude the atmosphere gases and carry the aerosol to the mass spectrometer, eliminating the requirement of the pressurised enclosing box. This later version showed reliable performance despite higher values for relative standard deviation (%) compared with standard ablation cell. While this set up allows mapping analysis, its main constraint is the need of a very flat and smooth surface to prevent the "curtain" gas to spill and keeping a good seal [10].

A third type of laser ablation open system have been developed to eliminates the needs of an ablation cell and allows a direct sampling in ambient atmosphere. By the mean of a membrane pump, the aerosol is extracted to a gas exchange device (GED) where the air is exchanged with argon before being introduced into the mass spectrometer [11,12]. Quantitative analysis on SRMs shows results in line with accepted values and results usually achieved with a closed cell configuration. This system coupled with an alternative ICP-MS interface and the addition of N_2 in the carrier gas has been applied to stalagmite analysis [13]. The performance of this set up allowed the quantification of REEs with a limit of detection in the (sub) ppb range.

Lately, another approach using portable laser ablation (pLA) have been developed to allow minimally destructive on-site analysis. This type of device typically includes a Nd:YAG pulsed laser system coupled with optic fibre and lens. The cell is located at the end and the of the lens tube and the sample ablation procedure require to place the module on the surface of the sample (i.e., with contact). By the mean of a membrane pump connected to the cell, the aerosol generated is sucked and transferred to a membrane filter. The filter can be subsequently digested and analysed with solution ICP-MS or ablated with a conventional LA-ICP-MS laboratory set up [14,15]. Alternatively, the pLA system can be connected to a GED device in an online configuration with the ICP-MS [16,17]. The main limitations of this approach include a LOD one or two order of magnitude higher than with conventional LA-ICP-MS sampling method and the use of 512 nm laser which has limited ablation efficiency on transparent or translucent materials. Adapting a 213 nm laser for the pLA approach is a promising alternative despite involving a trade-off in portability [18]. Lately, portable laser ablation method has been successfully used in heritage and archaeological science for bulk trace elements and isotope analysis on a wide range of materials (e.g. [19–23]).

The aim of the present study is twofold. Firstly, it aims at assessing the performance of the Artifact laser ablation platform. This system is made of two chambers: a self-seal open ablation cell enclosed in a large-volume chamber where the sample forms the base of the chamber, and a conventional "closed" ablation cell in a two-volume chamber (TwoVol2). The two systems use the same 193 nm laser for an optimal ablation efficiency on a wide range of materials with switching between the two cells achieved by a software-controlled mirror. The performance of the two cells is compared through the analysis of a set of glass standard reference materials (SRMs) commonly used in LA-ICP-MS analysis. The second aim of this work is to investigate the technology of Chinese-painted enamel copperware, specifically the composition of the polychrome paint layers of historical *Famille Rose* enamelled copperware. This study is the first to evaluate the capabilities of a commercially available open cell laser ablation system for LA-ICP-MS.

2. Materials and method

2.1. Materials

2.1.1. Standard reference materials

Eight glass SRMs were used to assess the performances and the accuracy of the open cell. The samples NIST 610 and NIST 612 are used in this study as calibration primary standards with the reference values published by Jochum et al. (2011) [24]. Secondary standards with different composition were also used: the Corning Museum Glass (CMG) A and D were developed to improve the analysis of historical and archaeological glass by providing samples with chemical composition similar to antique soda-lime silicate glass, and medieval potash-lime silicate glass, respectively [25,26]. The reference values used in this work are published in Vincenzi et al. (2002) [27] and Wagner et al. (2008) [28]. The DLH 1 glass sample is a high lead aluminosilicate glass (P&H Developments Ltd). The reference values have been recorded with SEM-EDS in Walton & Tite (2010) [29]. The British Glass Industry Research Association (BGIRA) 1, 2 and 3 glass samples were also included as secondary standards. The lead content in these 3 SRMs is 0.003 %, 3.25 %, and 9.06 % respectively. The values published in Adlington et al. (2020) [30] measured with LA-ICP-MS and EPMA were used as references.

2.1.2. The Famille Rose Chinese enamelled copperware sample set

Chinese decorative arts have been a source of intrigue and status in Europe for centuries, with demand increasing throughout the Ming dynasty (1368–1644) and continuing to the present day. By the 16th century export porcelain was a powerful factor in global trade dominating Western fashions in ceramics, resulting in intense competition and alchemical experimentation in Europe [31,32]. The term *Famille Rose* was coined by Albert Jacquemart in 1862 to describe a new enamel colour palette developed in China at the turn of the 18th century [33,34]. A broad range of polychrome overglaze enamels were developed through the coalescence of colour technology, raw materials, and firing techniques driven by the passion and patronage of emperor Kangxi (1662–1722) [35]. Painting in enamel arguably reached its pinnacle under the artistic direction of his successor, emperor Yongzheng (1723–1735). Hard paste porcelain was eventually developed in Europe by Johann Friedrich Böttger (1682–1719) after years of experimentation while incarcerated by Saxony Augustus II of Poland (1670–1733) and put into production at the Meissen factory in 1710 [36]. Jesuit Father Francois-Xavier d'Entrecolles (1664–1744) was sent on a mission to China in 1698. His now famous letters to Père Louis-Francois Orry in 1712 and 1722 [37,38] detail the manufacture of porcelain, glazes, enamels, and gilding in Jingdezhen. His letters were subsequently published in 1717 and 1735, after which potteries across Europe began to produce hard paste porcelain with elaborate overglaze enamel decoration. Manufacturing skills [39], recipes [40], processed enamels [41], and raw materials [42] continued to move between major production centres in the east and west throughout the 18th and early 19th century.

Early chemical analysis of Chinese enamels was carried out at the Sèvres porcelain factory on sets of prepared colours sent from Guangzhou by Joseph Ly in 1844 and Jules Itier in 1846, and on a further set sent from Jingdezhen by Rutherford Alcock in 1850 [43]. Scientific

techniques available at that time were predominantly destructive, resulting in the loss or significant alteration of those samples. A century later, Sir Harry Garner lamented that non-destructive methods were still not sensitive enough to identify colourants in his essay on *The Origin of Famille Rose* (1969) [33] Garner, a mathematician and former Chief Scientist at the Ministry of Supply 1949–53, was likely aware of contemporary advances in non-destructive analysis with X-ray Fluorescence (XRF) [44] and the potential application to the study of art. His experimental research on Chinese cloisonné [45] at the College of Aeronautics, latterly Cranfield University [46], is a surprising antecedent for the study of Chinese enamels at the institute.

In 2000, the technology of pink enamels was revisited in *What were the origins of Chinese Famille Rose?* by Kerr and Mills at the Victoria and Albert Museum [47,48]. Compositions of pink enamels on forty-eight objects in the museum collection were analysed with XRF, qualitative results were produced for major elements. These results highlight the limitations of spectroscopic X-ray analysis of high lead enamel-glass compositions. Recent studies have continued to drive the subject forward through a combination of analytical techniques and archival research. Among these studies, LA-ICPMS [49,50] is particularly promising for identifying the geological provenance of raw materials [42] and production centres [51].

To understand compositional variability in art objects, decoration on two Chinese painted enamel copperwares were analysed. They are Tray PCEDN1 and a Writing Set EPC11, both dating to the late Qianlong or Jiaqing period 1775–1820 (Fig. 1). The tray has a central "Hundred Antiques" motif depicting items for a scholar's desk and archaic bronzes [52,53]; a delicate pattern of gourds and lotus are painted on the reverse in blue. The interior rim is decorated with a narrow register of pink scrollwork followed and a more complex lotus pattern in black scroll with a purple ground, the underside of the rim with a cracked ice pattern in blue over green ground. Both sides of the rim have four reserve panels, the interior is embellished with polychrome flowers and the exterior in monochrome blue lotus patterns. The Writing Set is decorated with polychrome scrollwork, flowers, leaves, and a diaper pattern over yellow in a register above the feet. The set would have originally included and ink pot, candlestick, and pounce pot [54,55].

These two objects have undergone restoration work which allowed to sample two fragments (white and blue) on PCEDN1, and three fragments (white, turquoise, and yellow) on EPC11. The same colours have been analysed directly on the objects with the open cell system, with an additional examination of a pink area on each object.

2.2. Method

All experiments were carried out using the Artifact laser ablation system (Elemental Scientific Lasers, USA) equipped with a Coherent 193 ArF excimer laser. The Artifact is a dual-chamber platform comprising a large sample mounting chamber (maximum 600 x 600 x 600 mm) configured with a self-seal open cell (schematic cross-section in Appendix A – S.M. 1) that facilitates the analysis of large or irregular shaped objects without the need to sample them (as would be required for conventional laser ablation chambers). A secondary two volume chamber (TwoVol2 – closed cell) provides analysis of conventionally sized samples. In the model used for this study, sampling position in the large chamber equipped with the open cell, was controlled via a manually operated XYZ stage providing high precision control of 100 mm travel in X and Y, and 75 mm travel in Z with a straight-line accuracy of 10 μm. Samples were mounted on a sliding shelf, for accessibility across the entire 600 mm range, with fine final adjustment of the self-seal position so as to seal the chamber O-ring and provide haptic control over the pressure applied to the sample. The self-seal is a single volume chamber, sealing on a sample surface via a 12.7 mm silicone O-ring and between sample repositioning accommodates a working area of 4 x 4 mm. It is mounted on a hanging bracket to facilitate analysis of concave and convex samples. The aerosol is transported to the ICP-MS via a mixing bulb to smooth the transient signal and improve signal stability and mixing with argon as a makeup gas.

Each spot was ablated for 60 s with a laser fluence of 8 J/cm^2, a repetition rate of 15 Hz and a spot diameter of 70 μm. Gas blank was recorded during the 20 s warm-up time and the 20 s washout time. Helium was used as the carrier gas with a flow set up at 800 ml/min (operating parameters are summed up in Table 1). The samples and the SRMs were analysed in triplicate in the TwoVol2 chamber. In the self-seal chamber, the SRMs were also analysed in triplicate but the artworks were only analysed with a single spot to minimise the aesthetic invasiveness of analysis. During the analysis with the open cell, the quality of the seal was checked using an Agilent Electronic GC Leak detector to confirm a good seal between the O-ring and the sample surface.

All experiments were carried out using an Agilent 8900 ICP-QQQ-MS operated with a plasma power set at 1400 W, a plasma gas flow of 15 L/

Table 1
Operating parameters of the LA-ICP-MS system. * Integration time was reduced for some major elements.

ICP-MS: Agilent 8900		LA System: Artifact platform	
Mode	Single MS	Type	ArF
RF Power	1400 W	Wavelength	193 nm
RF Matching	0.95 V	Carrier gas (He) flow rate	800 ml/min
Sample Depth	7 mm	Fluence	8 J/cm^2
Plasma gas (Ar) flow	15 L/min	Frequency	15 Hz
Auxiliary gas flow	0.9 L/min	Laser beam diameter	70 μm
Integration time	20 ms*	Ablation time	60 sec
Time per sweep	1.15 s	Warm-up time	20 sec
# Isotopes measured	39	Wash-out time	20 sec

Fig. 1. Tray PCEDN1 (left) and Writing Set EPC11 (right) Chinese painted enamel on copper late Qianlong to Jiaqing period (1775–1820).

min, and an auxiliary gas flow of 0.90 L/min. The instrument was used in single MS mode with no cell gas. The ICP-MS was tuned on the glass SRM NIST612 to achieve high sensitivity and stability (RSD < 5 %). Plasma condition was monitored with the U/Th ratio (0.9–1.1) and the ThO/Th ratio was used to assess a low oxide level (ThO/Th < 0.01). The ICP-MS was setup in full-quant mode for the acquisition of 39 masses. The integration times was set to 0.02 s for most of the isotopes. The quantified data were calibrated using NIST 612 and NIST 610 as external standards and ^{29}Si as the internal standard following the sum normalization approach described by Van Elteren et al. (2009) [56] for ancient glass analysis.

3. Results and discussion

3.1. Comparison of the chamber performances

Performance of the two chambers of the Artifact system were compared using the glass SRMs NIST 612, NIST 610 and CMG A. Among the eight SRMs available for this study, these were selected because of their higher homogeneity. The graphs below display the results on a subset of 19 masses representative of the full range of isotopes measured in this study. This selection allows a better visualisation of the data. The results on the whole range of the masses measured are available in the Appendix A.

To assess the accuracy of the self-seal chamber, the five other SRMs (Corning D, DLH1, BGIRA 1, BGIRA 2, and BGIRA 3) were also analysed. The results are displayed on the full range of the 39 elements measured after calibration.

3.1.1. Sensitivity

Fig. 3**-A** shows the results for the sensitivity displayed as net counts (with background counts subtracted). For the three SRMs, a similar pattern is observed: the net counts recorded from the open cell is consistently lower than for the TwoVol2 chamber. For the same sample, the difference between the two chambers is quite constant across the range of masses selected. Comparing the three SRMs, the difference between the sensitivity of the two chambers is the highest in NIST 612 and smallest in CMG A. The graph of the net counts recovery rates (% of net counts recovered from the open cell compared to the TwoVol2 chamber) for the three samples (Appendix A – S.M. 1) shows that the values mostly range between 40 % and 60 % for NIST 612 and NIST 610, and between 50 % and 70 % for CMG A. The recovery rate calculated here does not seem to be correlated with the amount of element in the SRMs. Indeed, the calculated concentration for ^{93}Nb, ^{95}Mo, ^{139}La, ^{140}Ce, ^{232}Th and ^{238}U in CMG A is below 1 ppm while the published (and calculated) values for these same elements are between 30 and 40 ppm in NIST 612, and between 400 and 500 ppm in NIST 610.

This observation could be explained by the relationship between samples transparency and elemental fractionation. Several research [57–59] have documented the impact of sample transparency on the size of the particles in the aerosol. During ablation, transparent samples such as NIST 612, tend to produce larger particles than opaque samples which can be affected more by changes in transport efficiency. This hypothesis would explain the gradual improvement of net counts recovery rate between NIST612, NIST 610 and CMG A, following the increasing opacity of these samples. The same observation was made by Golitko *et al.* (2016) during the ablation of ceramic materials using an open cell system with a similar design. Here the setup configuration likely resulted in the lower transport efficiencies of the self-seal chamber; additional tubing length and additional connection points (relative to the TwoVol2) provides slow gas velocities and more potential dead volumes respectively for increased dropout of larger particles. The size of the cell and the nature of the sealing material could be another cause of the lower sensitivity of the open cell system. Bleiner & Gunther (2001) [60] showed the impact of the ablation volume on the dispersion and transport efficiency of the aerosol because of the aerosol-wall interaction. Moreover, the silicone O-ring is also prone to "trap" some large particles during the ablation. While a certain geometry is needed to accommodate the shape and the irregular surface of the objects to analyse, increasing the surface of contact between the silicone and the aerosol could also negatively affect the sensitivity of the open cell.

3.1.2. Precision

To evaluate the precision of the open cell, the net counts percent relative standard deviation values (%RSD) of the two chambers were plotted in Fig. 2**-B**. For NIST 612 and NIST 610, most of the %RSD values are below 3 % with little difference between the two chambers. The only exceptions are ^{118}Sn and ^{238}U in NIST 612. The higher %RSD values for ^{118}Sn in the two chambers could be explained by the higher volatility of the element and its comparatively low concentration in the transparent NIST 612. In CMG A, the %RSD values are above 3 % for ^{139}La, ^{140}Ce, ^{232}Th, and ^{238}U in the open cell only. This loss of precision is probably due to the very low quantity of these elements in the sample (measured < 0.7 ppm in this work), and consequently the low net counts recovered in the self-seal chamber as shown in Fig. 2**-A.**

3.1.3. Fractionation

Elemental fractionation occurring during LA-ICP-MS analysis can often be linked to the particle size diffusion and the characteristics of the elements considered (ionization potential, melting and boiling points, condensation temperature). It has been shown that elemental fractionation is dependent on the type of matrix ablated and the wavelength of the laser used [61]. Differences in the design of the ablation cells and the sample chambers can also contribute to fractionation by influencing the distribution of the aerosol particles during transport from the ablation cell to the ICP-MS [62,63,5]. The Fractionation index (Fi – [64]) can be used to assess the degree of fractionation between the open cell and the TwoVol2 chamber. It was calculated as the ratio of the averages of the ^{28}Si normalized signals of the first 30 s of ablation and the last 30 s of ablation. The results displayed in Fig. 3**-A** show a marginal fractionation effect in the two chambers with very little differences between them. Most of the Fi values range between 0.9 and 1.1. The higher fractionation indexes are recorded for ^{56}Fe in NIST 612 with the two chambers and on ^{140}Ce in CMG A with the self-seal chamber. The higher fractionation of iron on NIST 612 is explained by well-known polyatomic interference of ^{56}Fe with $^{40}Ar^{16}O^{+}$ and the low amount of Fe present in this sample. The higher Fi calculated for ^{140}Ce with the self-seal chamber is probably related to the very low amount of Ce present in CMG A (0.2 ppm measured with the closed cell) coupled with the already noted lower sensitivity of the open cell in this study. Looking at the whole range of the masses analysed (Appendix A – S.M. 3) the same observation can be made for the high Fi of Be in CMG A with the self-seal chamber (0.5 ppm measured).

3.1.4. Limits of detection

The limits of detection were calculated using the method from Pettke *et al.* (2012) [65] which is assuming a Poisson distribution rather than a normal distribution to accommodate very low count rates in the background. This method implies the calculation of sensitivity factor *S* determined using the element reference values published by Jochum et al. (2011) [24] for NIST 612 and NIST 610, and the values from Vicenzi *et al.* (2002) [27] and Wagner *et al.* (2012) [28] for CMG A. Fig. 3**-B** shows that for both chambers, the majority of the LOD values on the selected elements are below 1 ppm and below 0.1 ppm for most of the trace elements. Higher LOD values can be caused by a higher background signal coming from well-known polyatomic interferences such as ^{44}Ca with $^{12}C^{16}O_2$, or ^{56}Fe with $^{40}Ar^{16}O^{+}$. Generally speaking, the LOD values of the two chambers are very similar. It can be noted that some values from the open cell can be lower than for the TwoVol2 chamber in NIST 610 and CMG A, especially at the high mass end. This can be explained by the time needed to manually change the position of the laser spot on the open cell system, involving *de facto* a longer rinsing

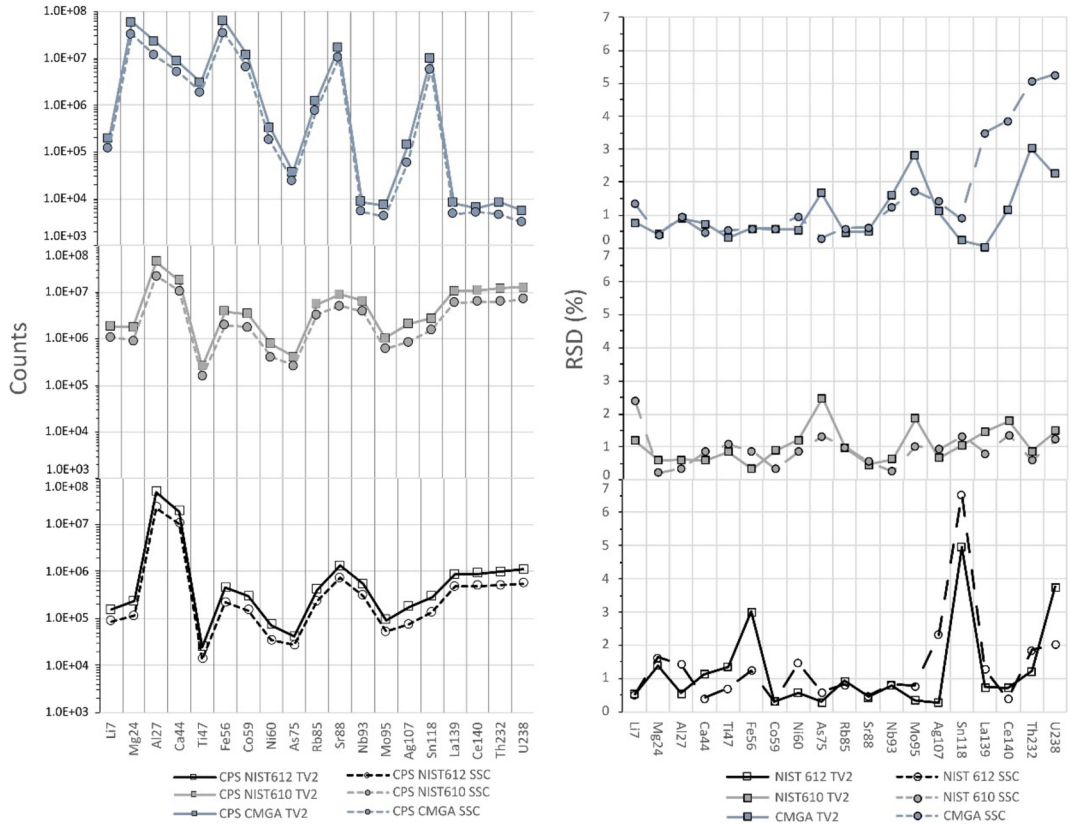

Fig. 2. Left (Fig. 3-A) displays the net counts on NIST 612, NIST 610 and CMGA for 19 masses (net counts are displayed on a logarithmic scale). Right (Fig. 3-B) displays the %RSD on these three samples.

time. Nevertheless, these results highlight the capabilities of the open cell to keep an air-tight atmosphere in the ablation cell during the analysis on a flat and smooth surface.

3.1.5. Accuracy

To assess the accuracy of the open cell, the quantitative results calculated on the NIST 612, NIST 610, CMG A, CMG D, BGIRA 1, BGIRA 2, and BGIRA 3 have been compared to the results obtained from the TwoVol2 chamber. Fig. 4 displays the difference (in percentage) between the two cells for the 39 elements measured during the analysis. Fig. 4**-B** shows the results for the samples NIST 612 and NIST 610 used for the calibration and re-processed as samples. On NIST 610 the deviation between the two cell is below 2 % for all the elements. On NIST 612, there is less than 5 % deviation between the two chambers on the vast majority of the elements. Only Cu, Zn, Sn, and Pb show a deviation between 10 and 15 %. Regarding the six secondary SRMs used in this study (Fig. 4**-A**), most of the elements show less than 10 % deviation. The high deviations (>10 %) observed on DLH1 are only observed on elements with calculated concentrations below 0.1 ppm (P, Zn, Rb, Mo, Cs and Au). On the three BGIRA samples, the higher deviations observed on some trace elements can also be caused by very low concentrations (Mo, Ag) or a possible heterogeneity in the samples (Cr, Zn, As, Sb, Pb). Overall, there is good agreement on the calibrated data of the secondary SRMs between the two chambers with few elements deviating more than 10 % when the concentration is above 0.1 ppm.

3.2. Results on the enamelled copperware

Both objects were initially formed in copper which was coated with a layer of white enamel. Once the ground layer was fired, polychrome enamels were hand painted onto the surface before re-firing to fix the decorative motifs. In this experiment, the opacified white enamel substrates and pink painted enamels on both objects were analysed. Yellow and turquoise green (the darker hue in the foliage) on Writing Set EPC11, and the blue on Tray PCEDN1 were also analysed.

Before calibrating the data acquired on the polychrome enamels, the time resolved analysis (TRA) spectra must be examined to assess the relative thickness of these layers and integrate the data corresponding to their ablation. Our results show that the white enamel is thick enough not to be ablated through its entire width (considering the instrumental parameters used in this work), but some painted layers are thin enough to be entirely pierced by the laser. Previous studies showed that the thickness of the painted enamels can range from 10 µm to 200 µm [66,50]. While the ablation efficiency depends on the material composition, striking differences can be observed on the time resolved analysis (TRA) spectra of the different painted areas. Among the 5 painted layers analysed, the turquoise was the only one which has not been ablated through the entire thickness of the layer. The pink layers present on the two samples seem to be the thinnest ones. On PCEDN1, the TRA spectra of Au and Sb raw counts (Fig. 5) sharply decreases after 11 sweeps (about 13 s of ablation) when the laser reaches the white enamel background. On EPC11, only 5 sweeps (about 6 s of ablation) were necessary before Au and Sn raw counts TRA spectra reach the white background. Beside their differences in chemical composition (discussed below), these two layers also have a different thickness highlighting some degree of technical heterogeneity.

For the blue layer on EPC11 (Fig. 5) the TRA spectra of Co and Sn raw counts are dropping after 9 sweeps (about 10.5 s of ablation) and stay low during the ablation of the white enamel. On the contrary, the yellow layer present on PCEDN1 seems much thicker. The TRA spectra of Sn and Zn raw counts is only dropping after about 33 sweeps (about 38 s of ablation). The relatively short time of ablation on the blue and pink layers involves a calibration on few data points (sweeps) on both the painted layers and the primary SRMs which can have an impact on the

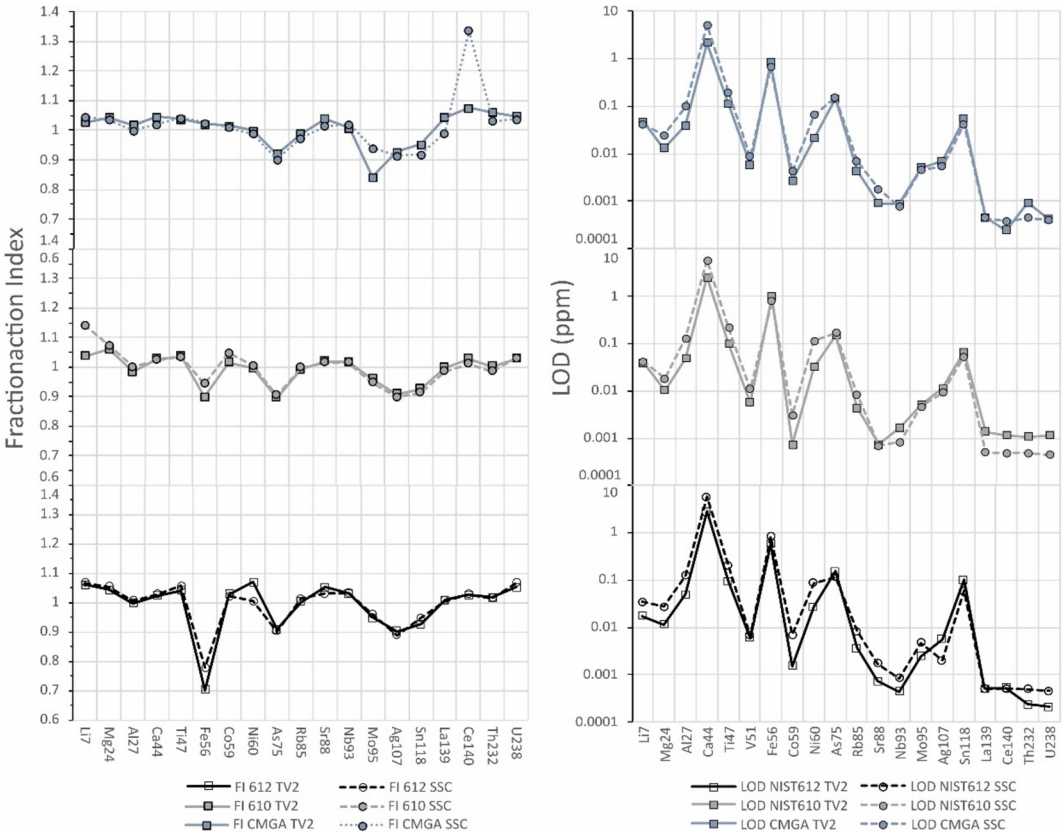

Fig. 3. Left (Fig. 3-A) displayed the fractionation index relative to ^{29}Si calculated on NIST 612, NIST 610 and CMG A. Right (Fig. 3-B) displays the limit of detection of the same three samples (LOD displays on a logarithmic scale).

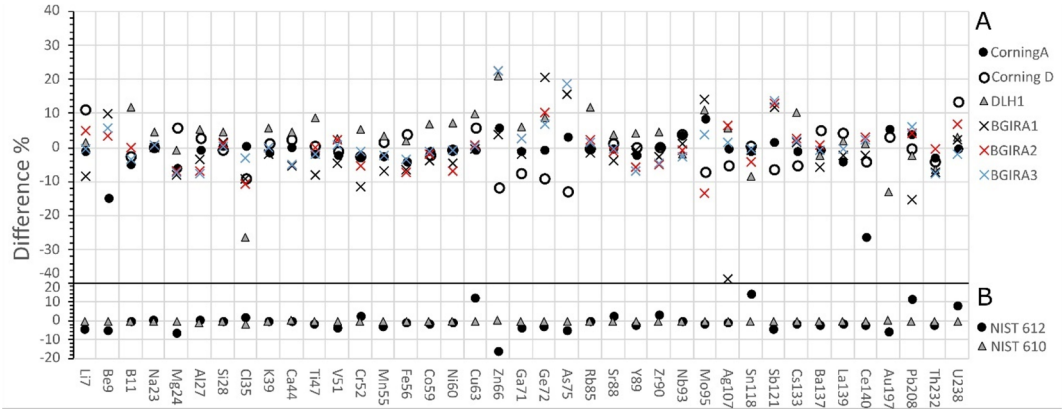

Fig. 4. Difference (%) between the elemental concentrations calculated with the self-seal chamber and the TV2 chamber after calibration. Fig. 4-B (bottom) shows the results for the external standards NIST 612 and NIST 610. Fig. 4-A (top) shows the results for the secondary standards.

precision and the accuracy of the results.

Results for the major components are presented in Table 2 as w% oxides. Results for colourants, minor, and trace elements are in Table 3 given as parts per million (ppm). The results are given for both the fragments analysed in the TwoVol2 chamber and the direct analysis on the artefacts with the open cell. Overall, differences can be noticed between the two types of samples analysed, mostly on the major element compositions. The compositional heterogeneity in *Famille Rose* enamel materials has already been assessed through the analysis of surface of cross-sections with SEM-EDS, pXRF and Raman spectroscopy [67,68,66,69]. This could be caused by the non-homogeneous dispersion of the opacifier and the colouring agents into the glassy matrix.

3.3. Discussion of enamelled copperware results

The term *Famille Rose* places emphasis on the introduction of pink enamels during the Kangxi period (1662–1722). The aesthetic change was in fact much broader including all the colours in this study except turquoise green. Before the Qing dynasty (1644–1911), Chinese enamelling technologies on ceramics and metal were divergent [70]. Kangxi directed the amelioration of enamelling technology at the turn of the 18th century, intentionally bringing together domestic and foreign materials and techniques. The term Huà Fàláng 畫琺瑯 directly translates as "painted enamel" and is used to describe decoration across fired media, demonstrating the conceptual and practical fusion of pyrotechnologies from this point in time [71].

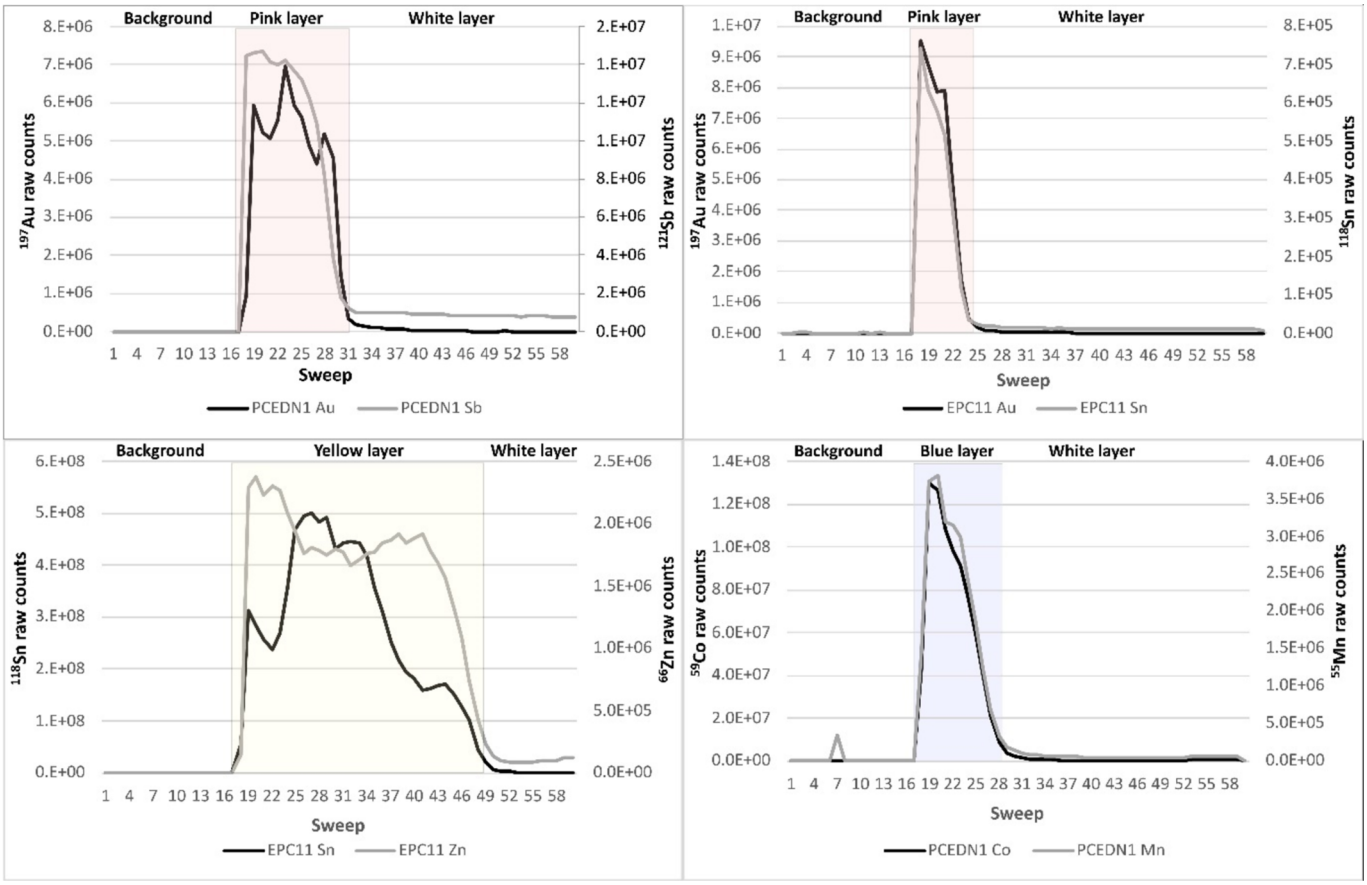

Fig. 5. TRA spectra acquired with the open cell on the pink, yellow and blue areas of the two objects analysed. Top Left – TRA for Au and Zn on PCEDN1. Top Right – TRA for Au and Sn on EPC11. Bottom Left – TRA for Sn and Zn on EPC11. Bottom Right – TRA for Co and Mn on PCEDN1.

Table 2
LA-ICPMS results for major elements in Chinese painted enamels presented as wt% oxides. DA: Direct analysis on the artefact with the open cell; F: Fragments analysed with the closed cell.

	Na_2O	MgO	Al_2O_3	SiO_2	K2O	CaO	TiO_2	MnO	Fe_2O_3	Sb_2O_3	PbO	B_2O_3	As_2O_3	SnO_2
PCEDN1-White DA	0.102	0.020	0.069	31.577	9.796	0.167	0.002	0.001	0.105	0.025	53.157	0.001	4.724	0.048
PCEDN1- White F	0.174	0.014	0.087	30.740	6.816	0.139	0.003	0.001	0.113	0.037	55.779	0.004	5.813	0.048
PCEDN-1-Blue DA	0.321	0.105	0.635	49.195	4.379	0.612	0.026	0.033	1.061	0.136	35.205	0.749	3.215	0.022
PCEDN1- Blue F	0.474	0.115	0.777	33.621	9.046	0.676	0.032	0.033	0.921	0.127	45.174	0.659	4.259	0.024
PCEDN1- Pink DA	0.172	0.092	0.495	39.615	9.542	0.263	0.019	0.029	0.177	0.309	47.612	0.115	0.254	0.009
EPC11-White DA	0.230	0.009	0.207	36.848	11.337	0.073	0.005	0.001	0.123	0.041	45.762	0.001	4.986	0.000
EPC11-White F	0.183	0.023	0.330	31.409	10.964	0.888	0.009	0.001	0.075	0.227	49.412	0.001	6.124	0.001
EPC11-Yellow DA	0.123	0.015	0.279	32.333	7.931	0.060	0.006	0.002	0.129	0.142	48.699	0.003	0.057	9.695
EPC11-Yellow F	0.130	0.015	0.256	30.080	8.463	0.079	0.007	0.002	0.121	0.168	51.651	0.003	0.052	8.160
EPC11-Turquoise DA	0.868	0.021	0.341	48.671	11.435	0.088	0.012	0.002	0.435	0.045	27.049	1.772	0.221	0.264
EPC11-Turquoise F	0.856	0.021	0.302	44.411	11.708	0.108	0.011	0.003	0.419	0.048	30.302	1.735	0.271	0.268
EPC11 – Pink DA	0.291	0.062	0.348	43.861	9.955	0.162	0.013	0.019	0.116	0.084	43.190	0.005	1.026	0.013

3.3.1. White enamel

The white enamel used to coat the copper substrates of both objects in this study are high lead silicates opacified with arsenic. The introduction of arsenic opacification was transformative to the *Famille Rose* palette because the white enamel could be blended with other colours to create countless semi-translucent variations. Both white enamels are high in potassium with low sodium and low stabilisers (Mg, Al, Ca) consistent with the results of previous elemental analysis of Chinese painted enamels. One of the advantages of LA-ICP-MS analysis is the ability to measure boron, recent research indicates that borax was used intermittently in the Qing dynasty [51,50]. The results of this experiment show that both objects belong to the borax free Guangzhou group, all objects analysed to date in this group are made in Western export styles.

3.3.2. Polychrome painted enamels

For discussion, the composition of each colour is compared to the white enamel layer below it.

Pink enamels have presented a long-standing analytical challenge due to the very small amount of material required for colouration in a high lead silicate matrix. Analysis with Microprobe and X-ray Fluorescence confirmed that this colour is produced with gold [47,72]. LA-ICP-MS is one of the few techniques that can accurately detect and quantify trace elements associated with manufacturing processes for this colour. As expected, gold was detected in both pinks, on Writing Set EPC11 at 1164 ppm and on Tray PECDN1 at 816 ppm. Both examples also have elevated amounts of chlorine in comparison to the white enamel substrate, likely associated with hydrochloric acid (3HCl) used to dissolve the metal into a colloidal suspension of nanoparticles. Slightly higher

Table 3
LA-ICPMS results for colorants, minor, and trace level Chinese painted enamel components in ppm. DA: Direct analysis on the artefact with the open cell; F: Fragments analysed with the closed cell.

	Li	Be	Cl	V	Cr	Co	Ni	Cu	Zn	Ga	Ge	Rb	Sr
PCEDN1-White DA	2.6	0.0	312.6	0.9	1.1	0.3	5.4	91.1	42.2	0.1	0.3	27.0	2.2
PCEDN1- White F	2.9	0.0	428.6	0.9	1.1	0.2	5.7	132.8	49.4	0.1	0.2	31.7	1.9
PCEDN-1-Blue DA	4.0	0.4	1407.4	9.1	3.9	10950.9	2321.8	794.9	2261.7	1.4	1.2	68.0	516.8
PCEDN1- Blue F	8.9	0.8	1437.6	8.7	3.7	9535.5	2311.1	590.1	1757.4	1.3	1.2	82.7	613.8
PCEDN1- Pink DA	5.4	0.2	1280.7	2.2	2.1	2.6	1.9	59.7	5156.2	0.8	0.5	46.0	6.7
EPC11-White DA	3.0	0.1	1049.7	0.7	1.3	0.2	3.1	251.9	22.8	0.2	0.6	61.0	1.5
EPC11-White F	2.4	0.1	1685.2	1.2	1.4	0.1	2.6	158.4	32.0	0.4	0.5	44.3	6.8
EPC11-Yellow DA	4.8	0.1	553.4	0.7	1.3	77.2	37.4	87.0	2274.3	0.4	0.6	33.2	2.8
EPC11-Yellow F	4.2	0.1	970.4	0.7	1.1	2.0	8.5	104.3	3090.1	0.4	0.6	34.2	2.3
EPC11-Turquoise DA	10.0	0.4	534.5	1.1	1.9	11.5	114.9	42652.9	25520.0	0.9	1.9	61.7	2.6
EPC11-Turquoise F	9.3	0.2	859.7	1.2	1.5	13.0	113.7	40217.7	31718.7	0.9	1.8	65.5	2.8
EPC11 – Pink DA	3.0	0.1	517.9	1.3	1.9	1.5	1.9	749.5	1695.8	0.5	0.6	60.0	4.0
	Y	**Zr**	**Nb**	**Mo**	**Ag**	**Cs**	**Ba**	**La**	**Ce**	**Au**	**Th**	**U**	
PCEDN1-White DA	0.2	0.6	0.1	0.1	144.7	0.3	2.0	0.2	0.3	0.0	0.1	0.03	
PCEDN1- White F	0.2	0.9	0.1	0.1	162.9	0.5	2.5	0.2	0.4	0.1	0.1	0.03	
PCEDN-1-Blue DA	13.8	68.1	1.0	57.7	288.0	1.8	11009.3	4.4	9.5	1.2	2.4	91.8	
PCEDN1- Blue F	17.1	88.1	1.2	57.8	263.5	1.5	12432.9	5.5	10.6	1.5	2.8	83.3	
PCEDN1- Pink DA	1.2	8.1	0.7	0.3	177.9	0.8	23.5	1.5	4.4	816.1	0.8	0.2	
EPC11-White DA	0.5	1.7	0.2	0.1	62.1	0.2	5.2	0.8	0.9	0.0	0.2	0.1	
EPC11-White F	1.1	4.6	0.3	0.0	95.3	0.3	10.0	1.8	3.1	0.0	0.4	0.1	
EPC11-Yellow DA	0.9	2.4	0.3	0.9	73.0	0.5	24.3	1.3	1.2	0.1	0.3	1.0	
EPC11-Yellow F	0.8	2.3	0.4	0.1	75.1	0.5	7.1	1.4	1.3	0.3	0.3	0.2	
EPC11-Turquoise DA	1.0	5.1	0.6	0.4	105.3	0.6	8.4	1.6	2.3	1.0	0.5	0.2	
EPC11-Turquoise F	1.0	8.7	0.6	0.4	100.8	0.5	8.7	1.5	2.3	1.7	0.4	0.2	
EPC11 – Pink DA	0.9	5.7	0.4	0.3	125.6	0.5	14.3	1.2	2.0	1163.9	0.4	0.2	

amounts of magnesium, boron, and silver were detected in the pinks, these elements are potential markers for historic glass making formulas. Tin and antimony are also associated with manufacturing processes; therefore, it is interesting to note that tin was only higher than the substrate on Writing Set EPC11, and antimony only higher on Tray PECDN1.

The yellow enamel on Writing Set EPC11 is clearly coloured with tin, whereas iron and antimony are at similar levels as the white layer below. This is consistent with previous studies on Chinese enamels from the Ming dynasty rather than imported European materials or manufacturing techniques [73]. There is a significant increase in zinc in comparison to the white substrate, and higher amounts of cobalt and nickel at trace level. Potassium is lower in the yellow painted enamel at approximately 8 % K_2O versus the white layer at 11 % K_2O. Boron is absent, and the proportion of SiO_2 and PbO remain relatively the same between the two layers despite the lower amount of potassium in the yellow. Turquoise green on Writing Set EPC11 is chiefly coloured with copper and zinc, accompanied by low iron; at trace level increases are seen in cobalt, nickel, silver, tin, and gold. We can see that turquoise green has a distinct composition from the yellow enamel because of differences in the proportions of tin and zinc, and the balance of the major glass formers (SiO_2 and PbO). Surprisingly, there is a significant amount of boron and lithium in the composition, indicating that borax was used as a raw material. The presence of borax in the turquoise green enamel is exciting because suggests that established colours were also refined during the 18th century.

Blue painted enamel on Tray PECDN1 has a complex combination of colourants and glass formers. The motif on the reverse of the tray analysed in the self-seal chamber is opaque with hints of grey and brown at the edges. The primary colourant is cobalt at roughly 10,000 ppm with manganese, iron, nickel, copper, zinc, and antimony contributing to the hue; increased molybdenum and uranium were detected at trace level. This combination of colourants and trace elements suggests that the enamel is coloured with a mixture of a manganese rich cobalt sourced in China, and an imported European cobalt [42,74]. The results confirm that the major opacifier is arsenic, but there is also increased phosphorus and calcium which could result from bone ash [67] added to achieve the grey-brown effect. In contrast with the white enamel layer, the blue is lower in lead, includes additional glass formers and fluxes including boron, barium, and sodium, and has higher levels of stabilisers in magnesium, aluminium, and calcium. The proportion of cobalt and barium in this example is in good agreement with a compositional group of Chinese painted enamels decorated in Western export styles dating to the late Qianlong-Jiaqing period (1750–1820) [66]. Barium is not a known accessory element in major cobalt ores [75]; therefore, it is more likely to be a component in the glassy matrix of a cobalt based pigment [76].

4. Conclusion

The work described above was able to give a very good comparison between the capabilities and limitations of the conventional TwoVol2 laser chamber and the open cell of the Artifact platform. The conventional laser chamber, at only 100x100 mm and 30 mm deep severely restricts the size of object that can be analysed. The open cell chamber under testing, at 600x600 mm and 600 mm deep, permits a much wider range of objects and opens a whole new range of possibilities for museums and other collections. A range of glass standards, all widely used in the analysis of ancient and historical glass, were used to compare the capabilities of the open cell to the conventional chamber. In terms of sensitivity, there was a significant loss of counts in the open cell compared to closed cell: typically, 40–70 % count rates were observed. Of these, the more opaque standards tended to have higher counts, which might be because transparent examples produce larger particles in the laser that do not transport so well. Despite the drop in counts observed, the precision of the final results in terms of the %RSD on the different count runs were very comparable between systems, with the open cell being less precise only on heavy elements in CMG A standard, probably because of their low abundance at < 0.7 ppm. In terms of accuracy, the deviation between the two cells was < 5 % for the great majority of elements on the NIST 612 standard and < 2 % on all elements for the NIST 610. Again, high deviations (>10 %) were almost always reserved for elements with very low concentrations (<0.1 ppm). In terms of LOD, the chambers were again comparable, with the LOD for the majority of elements at < 1 ppm, and < 0.1 ppm for trace elements such as La, Ce, U and Th and often an order of magnitude or two below this. Overall, this experimental work has shown that even though the open cell counts were lower than the conventional laser chamber, for

almost all operational purposes their performance was comparable. This means that very good analyses can be generated in the Artifact platform from objects of considerable size – a significant change for museums and collections wanting excellent analyses on large objects without subsampling and with very minimal damage to the objects. The fact that the whole analysis is carried out in an unpressurised container also greatly reduces the risk to glazed, glass and otherwise delicate objects compared to vacuum systems common in other techniques such as the scanning electron microscope.

The analyses carried out in the second part of the paper showed a case study of the application of the Artifact platform. Using TRA on two Chinese, polychrome enamelled copperwares, a tray and a writing set, layering within the enamels was able to be investigated over wide areas of the pieces where normal sampling would have been undesirable if not impossible. The coloured and white enamels were able to be accurately characterised and information about the heterogeneity of the layering and distribution of the enamels derived. The potential to work on multiple areas of a piece rather than drawing interpretations form a small fragment almost always derived from a rim and therefore of questionable representativeness is demonstrated. Overall, the Artifact platform open cell shows no disadvantage compared to the small chamber and a great deal more potential for the investigation of culturally valuable objects.

CRediT authorship contribution statement

Thomas Delbey: Writing – original draft, Visualization, Methodology, Investigation, Formal analysis, Conceptualization. **Dana Norris:** Writing – original draft, Investigation, Conceptualization. **David Douglas:** Writing – original draft, Visualization. **Andrew Shortland:** Writing – review & editing, Writing – original draft, Validation.

Declaration of competing interest

The authors declare the following financial interests/personal relationships which may be considered as potential competing interests: David Douglas reports a relationship with Elemental Scientific Lasers LLC that includes: employment. If there are other authors, they declare that they have no known competing financial interests or personal relationships that could have appeared to influence the work reported in this paper.

Appendix A. Supplementary data

Supplementary data to this article can be found online at https://doi.org/10.1016/j.microc.2024.112015.

Data availability

The data used in this paper are available on the Supplementary material files in the Appendix.

References

[1] L. Dussubieux, M. Golitko, B. Gratuze, Recent advances in laser ablation ICP-MS for archaeology, Springer, 2016.

[2] W. Devos, C. Moor, P. Lienemann, Determination of impurities in antique silver objects for authentication by laser ablation inductively coupled plasma mass spectrometry (LA-ICP-MS), J. Anal. At. Spectrom 14 (4) (1999) 621–626, https://doi.org/10.1039/a900073i.

[3] B. Wagner, W. Jędral, Open ablation cell for LA-ICP-MS investigations of historic objects, J. Anal. At. Spectrom 26 (10) (2011) 2058, https://doi.org/10.1039/c1ja10137d.

[4] K. Smith, K. Horton, R. Watling, N. Scoullar, Detecting art forgeries using LA-ICP-MS incorporating the in situ application of laser-based collection technology, Talanta 67 (2) (2005) 402–413, https://doi.org/10.1016/j.talanta.2005.06.030.

[5] M. Golitko, N. Sharratt, P.R. Williams, Open-cell ablation of Killke and Inka Pottery from the Cuzco area: museum collections as repositories of provenience information, in: L. Dussubieux, M. Golitko, B. Gratuze (Eds.), Recent Advances in Laser Ablation ICP-MS for Archaeology, Springer, 2016, pp. 27–52.

[6] S. Kosiba, K.E. Quave, N. Sharratt, M. Golitko, L. Dussubieux, P.R. Williams, Local knowledge and imperial art: A preliminary LA-ICP-MS analysis of clay preference and ceramic production practices in ancient Cuzco (Ca. 1100–1550 CE), J. Archaeol. Sci. Rep. 48 (2023) 103870, https://doi.org/10.1016/j.jasrep.2023.103870.

[7] Barringer A. (1980). US Pat., 4220414.

[8] P. Arrowsmith, S.K. Hughes, Entrainment and transport of laser ablated plumes for subsequent elemental analysis, Appl. Spectrosc. 42 (7) (1988) 1231–1239, https://doi.org/10.1366/0003702884430100.

[9] D. Asogan, B.L. Sharp, C.J. O' Connor, D.A. Green, R.W. Hutchinson, An open, non-contact cell for laser ablation-inductively coupled plasma-mass spectrometry, J. Anal. At. Spectrom 24 (7) (2009) 917, https://doi.org/10.1039/b904850b.

[10] M.B. Fricker, D. Gunther, Instrumentation, Fundamentals, and Application of Laser Ablation-Inductively Coupled Plasma-Mass Spectrometry, in: L. Dussubieux, M. Golitko, B. Gratuze (Eds.), Recent Advances in Laser Ablation ICP-MS for Archaeology, Springer, 2016, pp. 27–52.

[11] R. Kovacs, K. Nishiguchi, K. Utani, D. Günther, Development of direct atmospheric sampling for laser ablation-inductively coupled plasma-mass spectrometry, J. Anal. At. Spectrom 25 (2) (2010) 142, https://doi.org/10.1039/b924425e.

[12] D. Tabersky, K. Nishiguchi, K. Utani, M. Ohata, R. Dietiker, M.B. Fricker, I.M. De Maddalena, J. Koch, D. Günther, Aerosol entrainment and a large-capacity gas exchange device (Q-GED) for laser ablation inductively coupled plasma mass spectrometry in atmospheric pressure air, J. Anal. At. Spectrom 28 (6) (2013) 831, https://doi.org/10.1039/c3ja50044f.

[13] C. Wu, M. Burger, D. Günther, C. Shen, B. Hattendorf, Highly-sensitive open-cell LA-ICPMS approaches for the quantification of rare earth elements in natural carbonates at parts-per-billion levels, Anal. Chim. Acta 1018 (2018) 54–61, https://doi.org/10.1016/j.aca.2018.02.021.

[14] R. Glaus, J. Koch, D. Günther, Portable laser ablation sampling device for elemental fingerprinting of objects outside the laboratory with laser ablation inductively coupled plasma mass spectrometry, Anal. Chem. 84 (12) (2012) 5358–5364, https://doi.org/10.1021/ac3008626.

[15] R. Glaus, L. Dorta, Z. Zhang, Q. Ma, H. Berke, D. Günther, Isotope ratio determination of objects in the field by portable laser ablation sampling and subsequent multicollector ICPMS, J. Anal. At. Spectrom 28 (6) (2013) 801, https://doi.org/10.1039/c3ja30379a.

[16] M. Burger, R. Glaus, V. Hubert, S. Van Willigen, M. Wörle-Soares, F. Convertini, P. Lefranc, E. Nielsen, D. Günther, Novel sampling techniques for trace element quantification in ancient copper artifacts using laser ablation inductively coupled plasma mass spectrometry, J. Archaeol. Sci. 82 (2017) 62–71, https://doi.org/10.1016/j.jas.2017.04.009.

[17] S. Kradolfer, K. Heutschi, J. Koch, D. Günther, Tracking mass removal of portable laser ablation sampling by its acoustic response, Spectrochim. Acta B At. Spectrosc. 179 (2021) 106–118, https://doi.org/10.1016/j.sab.2021.106118.

[18] A. Knaf, P. Londero, J. Nikkel, R. Hark, A. Bezur, Novel portable laser ablation micro-sampling in cultural heritage, Microsc. Microanal. 27 (S1) (2021) 3014–3016, https://doi.org/10.1017/s1431927621010473.

[19] S. Seman, L. Dussubieux, C. Cloquet, T.O. Pryce, Strontium isotope analysis in ancient glass from South Asia using portable laser ablation sampling, Archaeometry 63 (1) (2020) 88–104, https://doi.org/10.1111/arcm.12618.

[20] A. Knaf, S.T. Habiba, J. Koornneef, A. Hertwig, J. Cárdenas-Párraga, A. García-Casco, G. Harlow, H. Schertl, W. Maresch, A. López Belando, C. Hofman, U. Brandes, G. Davies, Trace-elemental and multi-isotopic (Sr-ND-Pb) discrimination of jade in the circum-Caribbean: Implications for pre-colonial inter-island exchange networks, J. Archaeol. Sci. 135 (2021) 105466, https://doi.org/10.1016/j.jas.2021.105466.

[21] S.W. Merkel, P. D'Imporzano, K. Van Zuilen, J. Kershaw, G.R. Davies, "non-invasive" portable laser ablation sampling for lead isotope analysis of archaeological silver: A comparison with bulk and in situ laser ablation techniques, J. Anal. At. Spectrom 37 (1) (2022) 148–156, https://doi.org/10.1039/d1ja00342a.

[22] M. Numrich, C. Schwall, N. Lockhoff, K. Nikolentzos, E. Konstantinidi-Syvridi, M. Cultraro, B. Horejs, E. Pernicka, Portable laser ablation sheds light on early Bronze Age gold treasures in the Old World: New insights from Troy, Poliochni, and related finds, J. Archaeol. Sci. 149 (2023) 105694, https://doi.org/10.1016/j.jas.2022.105694.

[23] Kershaw, J., Merkel, S. W., D'Imporzano, P., & Naismith, R. (2024). Byzantine plate and Frankish mines: The provenance of silver in north-west European coinage during the long eighth century (c. 660–820). Antiquity, 98(398), 502-517. https://doi.org/10.15184/aqy.2024.33.

[24] K.P. Jochum, U. Weis, B. Stoll, D. Kuzmin, Q. Yang, I. Raczek, D.E. Jacob, A. Stracke, K. Birbaum, D.A. Frick, D. Günther, J. Enzweiler, Determination of reference values for NIST SRM 610–617 glasses following ISO guidelines, Geostand. Geoanal. Res. 35 (4) (2011) 397–429, https://doi.org/10.1111/j.1751-908x.2011.00120.x.

[25] R.H. Brill, A chemical-analytical round-robin on four synthetic ancient glasses, In IX Congrès International du Verre, Artistic and Historical Communications, 1972, pp. 93–110.

[26] L.W. Adlington, The Corning Archaeological Reference Glasses: New Values for "Old" Compositions. *Papers from the Institute of*, Archaeology 27(1): Art. 2 (2017) 1–8, https://doi.org/10.5334/pia-515.

[27] E. Vicenzi, S. Eggins, A. Logan, R. Wysoczanski, Microbeam characterization of Corning archeological reference glasses: New additions to the Smithsonian

Microbeam standard collection, J. Res. Nat. Inst. Stand. Technol. 107 (6) (2002) 719, https://doi.org/10.6028/jres.107.058.
[28] B. Wagner, A. Nowak, E. Bulska, K. Hametner, D. Günther, Critical assessment of the elemental composition of Corning archeological reference glasses by LA-ICP-MS, Anal. Bioanal. Chem. 402 (4) (2011) 1667–1677, https://doi.org/10.1007/s00216-011-5597-8.
[29] M.S. Walton, M.S. Tite, Production technology of Roman lead-glazed pottery and its continuance into Late antiquity, Archaeometry 52 (5) (2010) 733–759, https://doi.org/10.1111/j.1475-4754.2009.00506.x.
[30] L. Adlington, B. Gratuze, N. Schibille, Comparison of pXRF and LA-ICP-MS analysis of lead-rich glass mosaic tesserae, J. Archaeol. Sci. Rep. 34 (2020) 102603, https://doi.org/10.1016/j.jasrep.2020.102603.
[31] H. Crosby-Forbes, Yang-ts'ai, Rose Porcelains of the Ch'ing Dynasty. China Trade Museum, The Foreign Colors, 1982.
[32] Welsh, J. & Vinhais, L. (2015). *China of All Colours: Painted Enamels on Copper*. Jorge Welsh Research and Publishing.
[33] H. Garner, The Origins of Famille Rose, Transactions of the Oriental Ceramic Society 37 (1969) 1–36.
[34] A. Jacquemart, Histoire artistique, industrielle et commerciale de la Porcelaine, (1st ed.)., Techener, 1862.
[35] E. Curtis, Glass Exchange between Europe and China, Ashgate Publishing Limited, 2009, pp. 1550–1800.
[36] Gleeson, J. (1998). *The Arcanum*. Bantam.
[37] W. Burton, Letters of Père d'Entrecolles, in: Porcelain a Sketch of Its Nature Art and Manufacture, Cassell & Company Ltd., 1906, pp. 84–122.
[38] R. Tichane, Ching-te-chen: Views of a Porcelain City, Painted Post. (1983).
[39] Yang, B. (1987). A Brief Account of Qing Dynasty Glass. In C. Brown & D. Rabiner (Eds.), *Chinese Glass of the Qing Dynasty 1644-1911, The Robert H. Clague Collection* (pp. 71–86).
[40] W. Loibl, Itineraries of Glass Innovation, in: D. Von Kerssenbrock-krosigk (Ed.), Glass of the Alchemists: Lead Crystal - Gold Ruby 1650–1750, Corning Museum of Glass, 2008, pp. 63–74.
[41] E. Curtis, Vitreous Art: Colour Materials for Qing Dynasty Enamels, Arts of Asia 24 (6) (1994) 96–100.
[42] R. Giannini, I.C. Freestone, A.J. Shortland, European Cobalt sources identified in the production of Chinese Famille Rose porcelain, J. Archaeol. Sci. 80 (2017) 27–36, https://doi.org/10.1016/j.jas.2017.01.011.
[43] P. D'Abrigeon, The secret of colours: Chinese ceramics in China and Europe from the eighteenth century to the present, 5 Continents Editions, 2023.
[44] A.N. Shugar, J.L. Mass, Handheld XRF for art and archaeology, Leuven University Press, 2012.
[45] H. Garner, Chinese and Japanese Cloisonné Enamels, (2nd ed.)., Faber & Faber, 1971.
[46] R. Barker, Field of Vision: First Fifty Years of, University Press, Cranfield University. Cranfield, 1996.
[47] R. Kerr, What were the origins of Chinese Famille Rose? Orientations 31 (5) (2000) 53–59.
[48] A Study of Ruby-Pink Enamels on Chinese Porcelain: with a Comparison of Chinese Pink Glass and European Pink Enamels on Ceramics '99) (1999) 258–265.
[49] Y. Li, J. Zhu, L. Ji, Y. Shan, S. Jiang, G. Chen, P. Sciau, W. Wang, C. Wang, Study of arsenic in Famille Rose porcelain from the Imperial Palace of Qing Dynasty, Beijing, China. *Ceramics International* 44 (2) (2018) 1627–1632, https://doi.org/10.1016/j.ceramint.2017.10.084.
[50] L. Qu, X. Zhang, H. Duan, R. Zhnag, G. Li, Y. Lei, The application of LIBS and other techniques on Chinese low temperature glaze, MRS Adv. 2 (39–40) (2017) 2081–2094, https://doi.org/10.1557/adv.2017.85.
[51] D. Norris, T. Delbey, The influence of qing glass technology on qianlong and jiaqing painted enamel copperwares, J. Cult. Herit. 61 (2023) 160–167, https://doi.org/10.2139/ssrn.4231557.
[52] T.T. Bartholomew, Hidden meanings in chinese art, Asian Art Museum of San Francisco. (2012).
[53] M. Gillingham, Chinese Painted Enamel, Visual Art Productions Ltd., 1978.
[54] M. Rizk, Chinese painted enamels of the 18th century, The Chinese Porcelain Company. (1993).
[55] Woolley & Wallis, Asian Art I Tuesday 17th May 2016, Woolley & Wallis. (2016). https://www.woolleyandwallis.co.uk/departments/asian-art/aa170516/view-lot/170/.
[56] J.T. Van Elteren, N.H. Tennent, V.S. Šelih, Multi-element quantification of ancient/historic glasses by laser ablation inductively coupled plasma mass spectrometry using sum normalization calibration, Anal. Chim. Acta 644 (1–2) (2009) 1–9, https://doi.org/10.1016/j.aca.2009.04.025.
[57] M. Guillong, D. Günther, Effect of particle size distribution on ICP-induced elemental fractionation in laser ablation-inductively coupled plasma-mass spectrometry, J. Anal. At. Spectrom 17 (8) (2002) 831–837, https://doi.org/10.1039/b202988j.
[58] M. Guillong, I. Horn, D. Günther, A comparison of 266 nm, 213 nm and 193 nm produced from a single solid state Nd:YAG laser for laser ablation ICP-MS, J. Anal. At. Spectrom 18 (10) (2003) 1224–1230, https://doi.org/10.1039/b305434a.
[59] M. Gaboardi, M. Humayun, Elemental fractionation during LA-ICP-MS analysis of silicate glasses: Implications for matrix-independent standardization, J. Anal. At. Spectrom 24 (9) (2009) 1188, https://doi.org/10.1039/b900876d.
[60] D. Bleiner, D. Günther, Theoretical description and experimental observation of aerosol transport processes in laser ablation inductively coupled plasma mass spectrometry, J. Anal. At. Spectrom 16 (5) (2001) 449–456, https://doi.org/10.1039/b009729.
[61] Jackson, S. E. (2008). Calibration strategies for elemental analysis by LA-ICP-MS. In P. Sylvester (Ed.), Laser ablation-ICP-MS in the earth sciences: current practices and outstanding issues (pp. 169-188). (Short course series; Vol. 40). Mineralogical Association of Canada.
[62] S. Eggins, L. Kinsley, J. Shelley, Deposition and element fractionation processes during atmospheric pressure laser sampling for analysis by ICP-MS, Appl. Surf. Sci. 127–129 (1998) 278–286, https://doi.org/10.1016/s0169-4332(97)00643-0.
[63] D. Bleiner, A. Bogaerts, Computer simulations of sample chambers for laser ablation–inductively coupled plasma spectrometry, Spectrochim. Acta B At. Spectrosc. 62 (2) (2007) 155–168, https://doi.org/10.1016/j.sab.2007.02.010.
[64] B.J. Fryer, S.E. Jackson, H.P. Longerich, The design, operation and role of the laser-ablation microprobe coupled with an inductively coupled plasma-mass spectrometer (LAM-ICP-MS) in the earth sciences, Can. Mineral. 33 (2) (1995) 303–312.
[65] T. Pettke, F. Oberli, A. Audétat, M. Guillong, A.C. Simon, J.J. Hanley, L.M. Klemm, Recent developments in element concentration and isotope ratio analysis of individual fluid inclusions by laser ablation single and multiple collector ICP-MS, Ore Geol. Rev. 44 (2012) 10–38, https://doi.org/10.1016/j.oregeorev.2011.11.001.
[66] D. Norris, Technology and Conservation of Chinese Painted Enamels, Cranfield University, 2021. PhD Thesis.
[67] P. Colomban, Y. Zhang, B. Zhao, Non-invasive Raman analyses of Chinese huafalang and related porcelain wares. Searching for evidence for innovative pigment technologies, Ceram. Int. 43 (15) (2017) 12079–12088, https://doi.org/10.1016/j.ceramint.2017.06.063.
[68] P. Colomban, G. Simsek Franci, J. Burlot, X. Gallet, B. Zhao, J.B. Clais, Non-Invasive On-Site pXRF Analysis of Coloring Agents, Marks and Enamels of Qing Imperial and Non-Imperial Porcelain, Ceramics 6 (1) (2023) 447–474, https://doi.org/10.3390/ceramics6010026.
[69] D. Norris, D. Braekmans, A. Shortland, Technological connections in the development of 18th and 19th century Chinese painted enamels, J. Archaeol. Sci. Rep. 42 (2022), https://doi.org/10.1016/j.jasrep.2022.103406.
[70] Kerr, R., & Wood, N. (2004). *Science and Civilisation in China Volume 5: Chemistry and Chemical Technology, Part 12, Ceramic Technology*. Cambridge University Press.
[71] C. Shih, The Arrival of a New Colour Palette in Eighteenth-century Jingdezhen, in: P. D'Abrigeon (Ed.), The Secret of Colours: Chinese Ceramics in China and Europe from the Eighteenth Century to the Present, 5 Continents Editions, 2023, pp. 20–59.
[72] D. Kingery, P. Vandiver, The Eighteenth-Century Change in Technology and Style from the Famille-Verte Palette to the Famille-Rose Palette, in: D. Kingery, E. Lense (Eds.), Technology and Style (ceramics and Civilization), American Ceramic Society, 1985, pp. 363–381.
[73] J. Miao, B. Yang, D. Mu, Identification and differentiation of opaque chinese overglaze yellow enamels by raman spectroscopy and supporting techniques*, Archaeometry 52 (1) (2010) 146–155, https://doi.org/10.1111/j.1475-4754.2009.00466.x.
[74] R. Wen, The Cobalt Blue Pigment Used on Islamic Ceramics and Chinese Blue and White Porcelains, University of Oxford, 2012. PhD Thesis.
[75] Gratuze, B. (2013). Provenance Analysis of Glass Artefacts. In Modern methods for analysing archaeological and historical glass Volume I (pp. 311–343). Wiley.
[76] Q. Ma, D. Braekmans, A. Shortland, A.M. Pollard, The production and composition of chinese lead-barium glass through experimental laboratory replication, J. Non Cryst. Solids 551 (June 2020) 120409, https://doi.org/10.1016/j.jnoncrysol.2020.120409.

https://dspace.org/

Self-seal laser ablation open cell for trace elements analysis of full-size archaeological artefacts: application on Famille Rose enamel

Delbey, Thomas; Norris, Dana; Douglas, David; Shortland, Andrew J.

2024-12
Elsevier
https://doi.org/10.1016/j.microc.2024.112015
Delbey T, Norris D, Douglas D, Shortland A. (2024) Self-seal laser ablation open cell for trace elements analysis of full-size archaeological artefacts: application on Famille Rose enamel. Microchemical Journal, Volume 207, December 2024, Article number 112015

Downloaded from a DSpace repository. https://dspace.org/